Exergy Analysis of Ship Power Systems

Gordon G. Parker[a], Eddy H. Trinklein[a*], Rush D. Robinett III[a], Timothy J. McCoy[b]

[a]Michigan Technological University, Houghton, Michigan USA; [b]McCoy Consulting, LLC, Box Elder, SD USA
*Corresponding author. Email: ehtrinkl@mtu.edu

Synopsis

Ship subsystems and mission modules perform energy conversion during their operation resulting in a combination of electricity consumption, heat generation and mechanical work. These multi-physics subsystems often have opportunities for performing an energy storage role during their operation cycle. The kinetic energy stored in the rotating mass of a generator set or the electrical energy stored in a railgun pulse forming network are but two examples of energy storage aboard warships. Treating each subsystem as a disconnected entity reduces the potential for exploiting their inherent interactions and results in over- designed shipboard systems with excessive weight and volume. Exergy - the amount of energy available for performing useful work - provides a path for exploiting multi-physics energy flows. Utilizing the Second Law of Thermodynamics, by modeling and minimizing exergy destruction, a recent study, showed that exergy control increased the overall efficiency by 18% over traditional optimization techniques when applied to a terrestrial HVAC application. In this paper a notional, multi-physics ship power system is developed that explicitly captures the exergy flows. Particular attention is given to exergy destruction phenomena. Simulation of the system illustrates operational characteristics with greatest impact on exergy destruction highlighting areas for applying optimal, exergy-based control schemes. This approach will allow ship designers to minimize the size and weight of installed power generation, energy storage and thermal management systems, enabling the affordable implementation of advanced weapons and sensors.

Keywords: Exergy; Control; Pulsed Load; Energy Storage

1 Introduction

The US military has been pursuing the development of various electrically powered mission systems for a number of years. These systems include electromagnetic railguns, lasers, radio frequency weapons and solid-state radars (Kuseian, 2015), (Hecht, 2018), (O'Rourke, 2017). All of these new systems require large amounts of electric power compared to existing mission systems and the power is required in pulses of energy as opposed to a steady state draw. Because of the pulse-type nature of these new loads, power system designers are looking to energy storage to augment traditional generator sets for supplying the correct amount of power at the right time. The introduction of electrically powered mission systems also affects the ship's cooling plant. With efficiencies

Authors' Biographies

Eddy H. Trinklein Has both a B.S. and M.S. in Mechanical Engineering (2009 & 2011) and has worked at Michigan Technological University since 2011. Mr. Trinklein has worked on U.S. Navy projects for the past 7 years including control system development, motion sensor design and evaluation, scale model development leading to full-scale control system implementation and testing. His present research interests are ship mounted motion platforms designed to mitigate undesired payload motion. Prior to working for Michigan Tech, he was a fixture and machine designer at Key Design Inc.

Gordon G. Parker is the John & Cathi Drake Chair Professor Mechanical Engineering and co-Director of the center for Agile and Interconnected Microgrids (AIM) at Michigan Technological University. He specializes in control system design and optimization of mixed-physics dynamic systems. A key area of his research is the optimal control of power systems with particular attention given to networked topologies. Dr. Parker and his colleagues recently formed the Agile and Interconnected Micrgorid (AIM) Center to bring together faculty from Computer Science, Mathematics, Cognitive Sciences and Learning, Electrical and Computer Engineering and Mechanical Engineering to focus an interdisciplinary team on this technical area. As co-Director of AIM, Dr. Parker works with its 18 faculty to execute successful S&T projects with customers from DoD, DOE, and NSF. While at Michigan Tech he has mentored 50 graduate students, co-authored over 100 peer-reviewed publications and is a fellow of the Society of Automotive Engineers. Prior to his Michigan Tech appointment he was a senior member of the technical staff at Sandia National Laboratories in Albuquerque, New Mexico and a trajectory and control designer at General Dynamics Space Systems in San Diego, California.

Timothy J. McCoy is a consultant in the naval and marine industry. He was formerly the Director of the Electric Ship's Office (PMS-320) in Washington, DC where he was responsible for developing electric power, propulsion and control systems for the US Navy's fleet. There he initiated multi-million dollar international agreements for joint development of advanced ship power and control systems. Prior to entering government service, he worked in industry as a consultant, R&D Director and President of a defense contractor where he established a large R&D program for the marine, steel, renewables and oil & gas markets. Previously, he served active duty in the US Navy, where he developed integrated electric power and propulsion systems, control systems and designed several classes of ships. Dr. McCoy holds a BS in Mechanical Engineering from the University of Illinois; a Naval Engineer's Degree, SM in Electrical Engineering and PhD from MIT. He taught ship design and systems engineering while on the MIT faculty. A registered Professional Engineer, he is an IEEE Fellow and a member of ASNE. He is widely published and is an Adjunct Professor in the Electrical and Computer Engineering Department at Carnegie Mellon University.

Rush D. Robinett III is the Director of Research and the Richard and Elizabeth Henes Chair Professor of Energy Systems in Mechanical Engineering-Engineering Mechanics at Michigan Technological University. In January 2013, he retired from Sandia National Laboratories after 25 years of service as the Senior Manager of the Grid Modernization and Military Energy Systems Group focusing on the research and development of microgrids and networked microgrids. During his 25 year career, Dr. Robinett worked on ballistic missile defense, spacecraft systems, glide weapons, teams of robots, and renewable energy grid integration. He is an associate fellow of AIAA and has authored more than 180 technical articles, including three books and holds twelve patents. Dr. Robinett has three degrees in Aerospace Engineering: a BS and Ph.D. from Texas A&M University and an MS from the University of Texas at Austin.

http://doi.org/10.24868/issn.2631-8741.2018.025

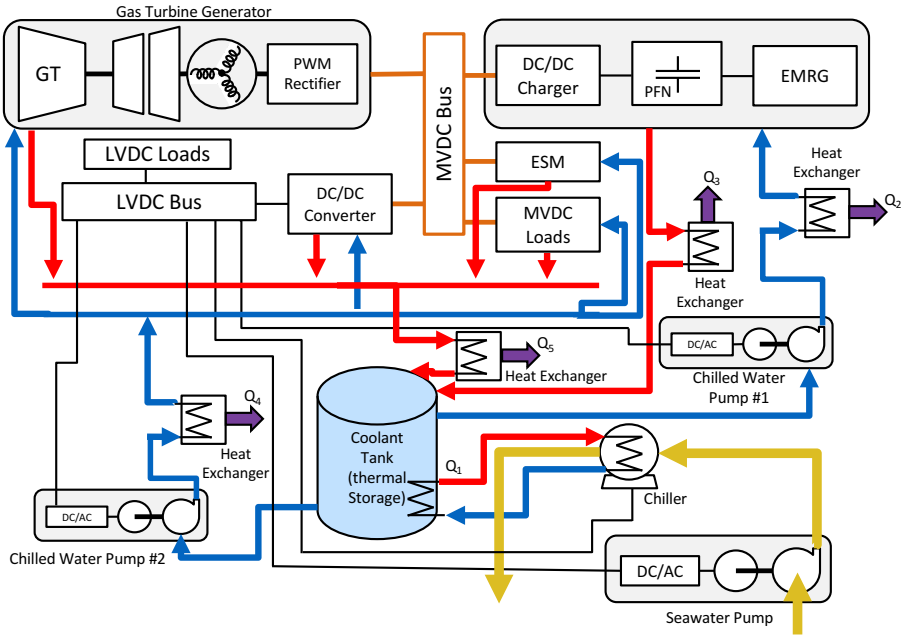

Figure 1: Electric Ship Model Configuration (Trinklein et al., 2018)

ranging from around 10-35%, much of the electric energy ends up as heat to be dissipated in the ship's cooling system.

The introduction of energy storage to the power grid opens up an entirely new set of control schemes that were previously not possible. Consequently, a number of researchers have investigated a variety of advanced control techniques including: linear quadratic regulators (Mills and Ashton, 2017), intelligent agents (Huang et al., 2007), (Patsios et al., 2012), market-based approaches (Zhang and Cramer, 2017) and distributed control (Monti et al., 2005) many others. Common to most previous work is that the power grid is viewed in isolation, with subsystem focused optimization. The present work takes a multiphysics approach to optimization of both the electric power and the cooling systems simultaneously. By considering the ship as a complete 'system of systems', there is potential that the main power and cooling systems could be reduced in size while still meeting the same performance requirements. This requires a methodology to account for energy loss mechanisms in multiphysyical systems, namely thermal, electrical and mechanical systems. Exergy destruction is a thermodynamic generalization of the concept of 'dissipation' or 'losses' in electrical, mechanical and thermal systems which is a scaled version of irreversible entropy production. Exergy destruction is a measure that is often used to evaluate the efficiency of thermodynamic systems or processes. Capturing the major exergy destruction terms requires models which are capable of calculating the exergy destruction processes within each component. Exergy models for a ship example were recently developed by Trinklein et al. (2018). This paper develops the models further with the inclusion of electrical energy storage on the medium voltage bus and shows the results of exergy destruction control optimization.

2 System Description

The electric ship model is shown in Figure 1, highlighting the level of interconnectedness of the subsystems and relative level of complexity. A summary of the model is given below where each subsystem is explained in brief detail, while the electrical storage and its control model is explored in depth.

2.1 Gas Turbine

The 19.8 MW version of General Electric LM2500 gas turbine provides the energy for all the ship subsystems. Its model was implemented in MATLAB/Simulink as a C-coded S-function based on the equations developed in Doktorcik (2011). The exergy destruction associated with burning fuel was added as an output. A stable underdamped PID controller was responsible for maintaining a rotational speed of 377 rad/s or 3600 RPM. A limitation of the physical turbine is how quickly the loading can change before unstable operation can occur, such as flame-out, surging and stalling. To avoid these conditions, ramp rates of 0.5 MW/s or 30 MW/min are specified by the OEM. In the turbine model, the ramp rate limits can be exceeded and are enforced by preventing load conditions to change above the ramp rate limits.

http://doi.org/10.24868/issn.2631-8741.2018.025

2.2 Lumped Parameter Generator, Neutral Point Clamped Rectifier and 6 kVDC Bus

The simulation of long duration studies, on the order of minutes to hours, requires model simplification to enable simulation runs above realtime speed. This was accomplished by combining the behavioral characteristics of the AC generator, Neutral Point Clamped (NPC) active rectifier, and the DC bus into a lumped parameter model. The model was fit to a detailed switching mode model where the boundary conditions of generator rotational speed, electrical torque, output bus voltage and current and losses were matched. The detailed model was comprised of a 240 Hz high frequency generator producing 6900 VAC and rated at 22 MVA, based on parameters given in Calfo et al. (2008). An IEEE type 1 (D. C. Lee , Editor , 2006) exciter was used to maintain the AC output voltage. Rectification to 6 kVDC was accomplished by a three level NPC fed through a wye to delta transformer sized to produce a modulation index of 0.8. The output capacitors on the NPC form the 6 kVDC bus. Two passive loads were integrated into the model representing base loads while providing numerical stability: (1) 1 MW attached to the AC output of the generator and (2) 0.2 MW attached to the NPC terminals.

2.3 Medium Voltage Loads

Attached to the 6 kVDC medium voltage bus are five load types. First, a passive resistive load of 1 MW used to shift the based load of the turbine. Second, a controllable load implemented with a current source to ground, presently set to zero. Third, a DC/DC converter feeding the 1 kVDC low voltage bus. Fourth, energy storage which can act as a load or source. Fifth, a pulsed load representing the dominant system load and described in more detail below.

2.4 Pulse Load

A 30 MJ muzzle energy electromagnetic railgun (EMRG) was implemented based on work by Deadrick et al. (1982) and Bernardes et al. (2003). The railgun consists of three components: (1) a buck/boost charger, (2) a 70.2 MJ capacitive energy storage bank, and (3) the railgun circuit elements. Contactors separate the railgun from the capacitor bank and the capacitor bank from the medium voltage bus. This allows for firing the railgun by isolating the capacitor bank from the main bus thereby avoiding a sharp pulse load that would be noticed across the broader electric grid. Loading on the ship's grid is dependent on the charging rate of the capacitor bank and is therefore controllable through the buck boost charger's control system. Operation of the railgun system, considering a discharged capacitor bank, begins by closing the charge contactor while the charger output is commanded to output zero volts. Next, the charger output voltage is increased to achieve a desired charging load current profile on the medium voltage bus side. The charging profile is precomputed to achieve the desired voltage of 7500 VDC at an energy capacity of 70.2 MJ. Charging completes by disconnecting the charge contactor and then setting the charger voltage output back to zero. Finally, the firing contactor is closed to discharge the capacitor bank and convert stored electrical energy into kinetic energy of the projectile. The conversion of electrical energy into kinetic energy was assumed to be 42.7 %, (Bernardes et al., 2003). The remaining energy was converted to ohmic heating in the rails, 37.4 %, and distributed in the wiring, inductors, contactor and diodes, 19.9%

2.5 Buck Converter

The 1 kVDC low voltage bus is supplied by a buck converter attached to the medium voltage bus. Its controlled with a PID with feed forward designed to maintain a constant voltage. Losses within the system are comprised of switching and conductive losses in the power electronics and ohmic losses from the passive devices.

2.6 Low Voltage Loads

On the low voltage bus are the ship service loads consisting of a passive load of 333 kW, and three pumping loads from the thermal management system along with the chiller load.

2.7 Thermal Modeling and Exergy Destruction

The thermal objectives are to regulate the internal energy of the rails and a lumped thermal mass representative of all the electronics. The thermal management system uses a chiller, modeled as a single monolithic device, to extract energy from a coolant tank, shown in Figure 1. The coolant tank pumps cool water to the thermal loads and receives the returning hot water. Differential equation models of the tank coolant, heat exchangers, and both thermal loads are used along with exergy destruction calculations. Exergy destruction occurs due to conduction and convection in the thermal masses, the coolant tank and the seawater side of the chiller. Additional exergy is destroyed due to the mixing of multiple temperature water flows into the tank. A detailed description of the exergy destruction submodels model is given in Trinklein et al. (2018).

http://doi.org/10.24868/issn.2631-8741.2018.025

2.8 Energy Storage Model

A supplementary energy storage device, separate from the railgun capacitor storage bank, is attached to the medium voltage bus (V_{MVDC}). Its proper use and sizing permits higher firing rates by allowing the railgun capacitor bank to charge without exceeding the turbine's ramp rate. It's modeled as shown in Figure 2 using a controlled current source behind a resistive loss similar to Wilson et al. (2012). The series resistance, R_{esr}, represents a lumped loss term of the energy storage system and contributes to exergy destruction through Eq. 1, where I_{batt} is the commanded current. The storage voltage, V_{batt}, is a function of state of charge (SOC). The device's SOC is given in Eq. 2 (Coleman et al., 2007), where C is the storage capacity in Amp-Hours which were later converted to Mega-Joules, SOC_{init} is the initial SOC and I_{batt} is the current integrated from the start of the simulation t_0 to the end t_1. This model approach was used to 1) have an agonistic storage element with respect to storage type and 2) to study storage requirements in terms of energy capacity, power delivery and power rate.

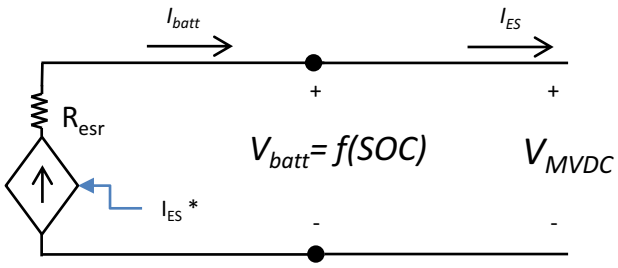

Figure 2: Energy Storage Implementation

$$P_{esr} = I_{batt}^2 R_{esr} \tag{1}$$

$$SOC = 100\left(1 - \left[\frac{1}{3600C}\int_{t_0}^{t_1} I_{batt}(t)dt + \frac{SOC_{init}}{100}\right]\right) \tag{2}$$

The feed forward storage command, I_{ES}^*, is generated from the desired charge profile, I_{Charge} and the profile error value $I_{Charge,Error}$ and multiplied by a gain factor, $P_{FF,CH}$ that controls the amount of storage contribution applied.

$$I_{ES}^* = P_{FF,CH}\left(I_{Charge} - I_{Charge,Error}\right) \tag{3}$$

It should be noted that energy storage management was not addressed here. This is an important consideration for practical implementation and is currently under investigation.

3 System Simulations

Using the model parameters from Trinklein et al. (2018) the minimum firing period, without supplementary storage, was 33 seconds due to the turbine's ramp rate limit. The analysis below focuses on decreasing the firing period using supplementary storage and the effect this has on exergy destruction.

3.1 Increasing Pulse Rate with Electrical Energy Storage

A procedure for determining the minimum amount of supplementary storage needed to achieve a desired firing rate is described below such that the operational constraints of Table 1 are not violated and in particular the *Turbine Ramp Rate* of ± 0.5 MW/s.

The following system operating limits were selected to be general parameters and not specifically tied to a single design. The 6 kVDC and 1 kVDC bus voltages are allowed to exceed their *Nominal Limits* up to their *Transient Limits* for at most *Transient Recovery Time* seconds. The *Railgun Capacitor Bank Voltage* must achieve 7500 ± 1 VDC before firing. The *Railgun Body Temperature* must stay below 130 C. The thermal system's *Water Mass Flow Rate*, a primary parameter for transferring hear, was limited to 2 kg/s The thermal system also had

http://doi.org/10.24868/issn.2631-8741.2018.025

Table 1: System Operating Limits

Description	Value	Units
Turbine Ramp Rate Limits	−0.5 to 0.5	MW/s
6 kVDC Bus Voltage Transient Limits	5100 to 6600	VDC
6 kVDC Bus Voltage Nominal Limits	5400 to 6330	VDC
1 kVDC Bus Voltage Transient Limits	900 to 1100	VDC
1 kVDC Bus Voltage Nominal Limits	940 to 1060	VDC
Transient Recovery Time	0.1	sec
Railgun Capacitor Bank Voltage Range	7499 to 7501	VDC
Railgun Body Maximum Temp.	130	°C
Water Mass Flow Rate Limit	2.0	kg/s

several fixed parameters including the seawater inlet temperature of 25C, and the chiller supply temperature of -15C. The chiller supply temperature is considered the internal coolant temperature and not the chilled water output temperature as supplied throughout contemporary ships today.

A generalized single cycle of the capacitor bank charging current is given in Figure 3. The overall time period between shots is noted as F_P beginning with the start of a charging cycle. In this case, the rise and fall, dimension "a" of the trapezoidal profile is symmetrical and accomplished using a fifth order polynomial, as found in (Biagiotti and Melchiorri, 2008), that begins and ends with zero slope. The constant current section is denoted as "d" and can be reduced down to a single sample period of the simulation (0.001 sec) as a minimum value. The peak value associated with the constant current section is given as "c". Finally, the fire command is delayed from the next charging cycle by dimension "d". This general shape was optimized to limit turbine ramp rate during the railgun capacitor charging cycle.

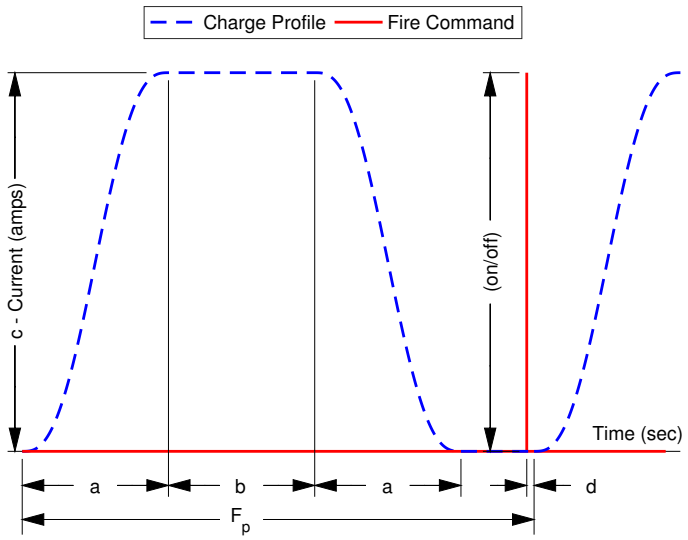

Figure 3: Fifth Order Polynomial Trapezoidal Charge Profile

Selection of required storage was done in two optimization steps. First, the railgun capacitor bank's charge profile was found that met the capacitor bank voltage requirements of 7500 vDC while also minimizing the "a" duration with also minimizes turbine ramp rate. Secondly, storage was added to bring the ramp rate violation within 0.5 MW/s; further details of each run are described next.

In the first set of optimization runs, the free variables were the "a" the ramp or down portion of the charge profile and "c" the maximum current during the constant charge portion of Figure 3. The fire period, "Fp" was varied between 6 and 33 seconds and "b" was computed based on the present "a" value and a fixed 0.25 sec delay between the charging profiles, defined as $(2a+b)$, for each fire period. Limits were applied to the computed "b" to always be greater than 0.01 seconds. Similarly, the "a" values were constrained to have a greater than 0.01 second transition time. Turbine ramp rate limits were removed because storage was not yet added. To speed the solution

http://doi.org/10.24868/issn.2631-8741.2018.025

the runs were sequential and a previous solution used for the next test case.

In the second set of optimization runs, storage was added, through the gain parameter $P_{FF,CH}$ of Eq. 3 until ramp rate was brought within the limits. This was done through the feed-forward term of the storage command used to drive the capacitor charge command, as described above. Another way to consider $P_{FF,CH} * 100$, is the percentage of pulsed load handled by the storage system and $1 - P_{FF,CH} * 100$ is the percentage handled by the turbine directly. The simulation duration was varied to allow 10 full charge and fire cycles to occur after which the simulation was halted and various final parameters were recorded. The recharging of storage was not a concern in this paper but would need to be dealt with eventually after a fire sequence has occurred. Furthermore, the cooling system and railgun temperatures either reached their maximum value or achieved a steady state limit cycle behavior as the fire period was relaxed. For the 6 second case a peak railgun body temperature 121° C was observed and lower temperatures were recorded for longer fire periods.

The results of the dual optimization runs are plotted in Figure 4. Exergy destruction throughout the system is given without the contribution from the turbine, as the turbine 1) dominates the response and 2) is not reducible unless electrical loading is lowered. For fire periods of 6 to 21 seconds, the destruction increases exponentially, with decreased fire period. For longer fire periods beyond 21 seconds, the destruction stabilizes around 38 MJ for 10 shots of the railgun. This suggests that fire rates above 6 seconds would lead to further exergy destruction. Secondly, that if fire rates in the 33 to 21 second range were acceptable from a performance perspective, the system efficiency could be improved.

Both peak power delivery and expended energy of the energy storage were recorded in Figure 4, and reduce as fire period increases. Required storage energy content has a bilinear characteristic which has a knee at 21 second fire period. The bilinear characteristic is likely tied to the thermal time constants associated with the rails, auxiliary electronics, or coolant. The bilinear trend is not observed for pear power delivery required which is tied to the charge profile maximum current.

The percentage of the charging load delivered by the storage system is also plotted. At a 6 second period, the turbine is completely unable to handle the ramp rates required to fully charge the energy storage. This suggests that fire periods shorter than 6 seconds would also need storage to achieve, where the pulse load is handled solely by storage. For fire periods longer that 33 seconds, storage is not needed and this is consistent with the findings in (Trinklein et al., 2018).

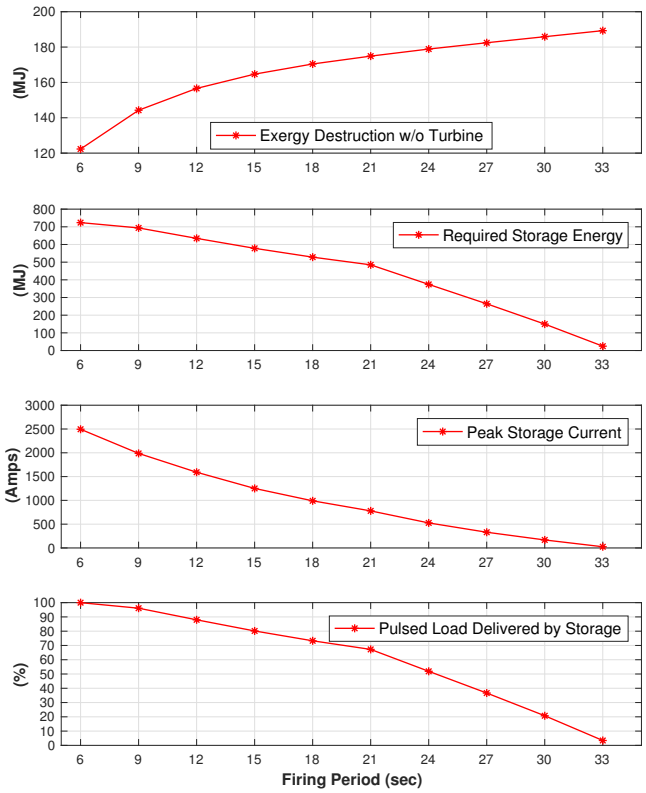

Figure 4: Total Exergy Destruction for Ten Pulses, Required Electrical Storage, and Percentage of Load Handled by Storage

http://doi.org/10.24868/issn.2631-8741.2018.025

Table 2: Exergy Destruction Component Contribution

Shot Period (Sec)	Storage Size (MJ)	Exergy Destroyed [MJ], (% total)				
		Chiller	Tank	Sea Water	Rails	Other Loads
6	723.7	[38.0], (31.1)	[35.2], (28.8)	[17.6], (14.4)	[17.2], (14.1)	[14.3], (11.7)
18	528.3	[65.4], (38.4)	[50.9], (29.9)	[32.2], (18.9)	[13.0], (7.6)	[8.9], (5.2)
33	24.7	[75.3], (39.8)	[55.5], (29.3)	[40.6], (21.5)	[10.0], (5.3)	[7.8], (4.1)

To explore why the exergy destruction increases with longer fire periods three simulation runs have been plotted in Figure 5. The top of Figure 5 shows the total exergy destruction which occurred for the 6, 18, and 33 second fire periods, suggesting a trade-off between bulk electrical storage size and exergy destruction. The exergy destruction rate was higher for the 6 second case as compared to the 18 and 33 second cases and exergy destruction lowered as fire period decreased. However, this view is incomplete without considering the destruction mechanisms and thermal management. By observing the railgun body temperature for the three cases, given in the bottom of Figure 5, the temperatures are lower for longer fire periods. Since the thermal system was a static size in this study, the system can achieve lower temperatures when less energy per unit time is applied. While not studied here, the authors suspect that if similar cooling temperatures were required for the 6 second period, as obtained for the 33 second case, the exergy destruction would be significantly higher for the 6 second case.

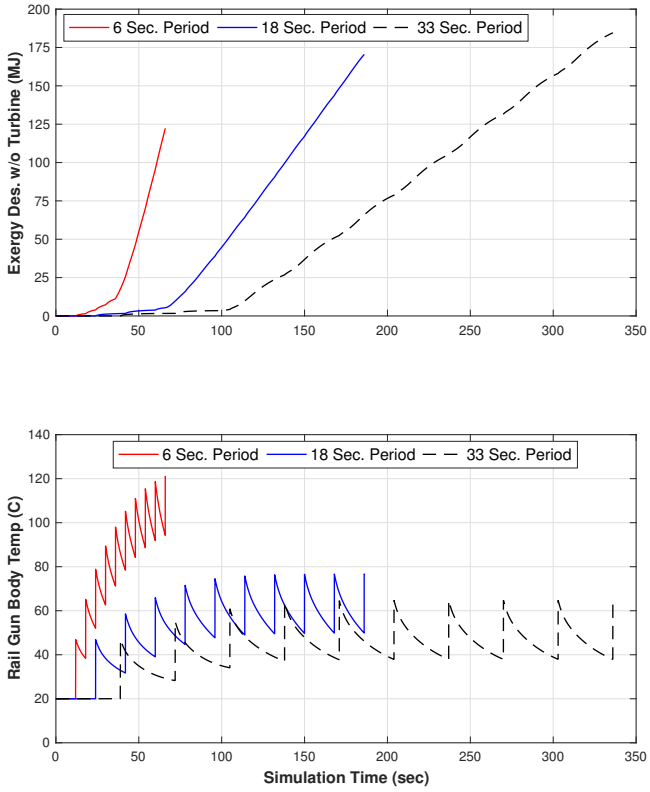

Figure 5: Total Exergy Destruction without Turbine and Railgun Body Temperature for 6, 18, and 33 second fire periods

Additionally, the exergy destruction contributions of the chiller, tank, sea water loop, railgun's rails, and the other electrical loads were complied in Table 2 for the 6, 18, and 33 second cases. The chiller and tank represent the largest contributors, with the exception of the turbine, to system wide exergy destruction. Contribution from the tank is constant at 29.3 % of the total while the chiller's contribution increased with shot period. A similar trend to the chiller was observed on the sea water cooling loop. The opposite trend is found with the rails and other loads were exergy destruction lowers as a percentage of the total as shot period increases. A fitting explanation for the other loads trend is that the electronics were exercised less at longer fire periods resulting in lower ohmic heat generation, hence lower exergy destruction.

http://doi.org/10.24868/issn.2631-8741.2018.025

4 Conclusions and Further Research

With the addition of storage, the railgun fire rate was improved from 33 seconds as the baseline case to 6 seconds. For fire rates in the 6 to 21 second period the exergy destruction had an exponential trend. For 21 to 33 second fire periods, exergy destruction was nearly flat.

To achieve a 6 second fire period, a supplementarity energy storage size of roughly 750 MJ with a 6000 volt supply voltage and a current capacity of 2500 amps is required to fire ten sequential shots. The storage system would be fully responsible for supplying the charging current for the railgun capacitor energy storage. After the fire sequence, both the energy storage would need to be brought back to its initial storage state to allow another fire sequence.

A tradeoff between total exergy destruction and installed electrical storage was observed where as storage was increased exergy destruction decreased. This trend is more complicated since it is tied to the cooling system performance and desired operating temperature of the railgun. An investigation is required for non-static cooling size where railgun temperatures are kept constant while comparing exergy destruction.

In future work, an additional gas turbine could be added to improve ramp rate limits and to further explore system optimization under varying loading conditions. The trapezoidal charge profile, with fifth order polynomial transitions, provides a starting place for an optimal railgun charging profile. By optimizing both the bulk energy storage along with the charge profile utilizing an arbitrary curve could provide further performance improvements. Feed forward commands to the cooling system could also be used to reduced exergy destruction and further investigation is required. The coolant system is a significant portion of the total exergy destruction of the ship system and changes to coolant inlet temperature or tank temperature set points require further study.

Acknowledgement

This work was supported by the U.S. Department of Defense, Office of Naval Research under the award No. N00014-16-1-3044. The views and conclusions contained in this document are those of the authors and should not be interpreted as representing the official policies, either express or implied, of the Office of Naval Research or the U.S. Government.

References

Bernardes, J. S., Stumborg, M. F., Jean, T. E., Jan 2003. Analysis of a capacitor-based pulsed-power system for driving long-range electromagnetic guns. IEEE Transactions on Magnetics 39 (1), 486–490.

Biagiotti, L., Melchiorri, C., 2008. Trajectory planning for automatic machines and robots. Springer Science & Business Media.

Calfo, R. M., Poole, G. E., Tessaro, J. E., 2008. High frequency ac power system. Naval Engineers Journal 120 (4), 45–54.

Coleman, M., Lee, C. K., Zhu, C., Hurley, W. G., Oct 2007. State-of-charge determination from emf voltage estimation: Using impedance, terminal voltage, and current for lead-acid and lithium-ion batteries. IEEE Transactions on Industrial Electronics 54 (5), 2550–2557.

D. C. Lee , Editor , April 2006. IEEE recommended practice for excitation system models for power system stability studies. IEEE Std 421.5-2005 (Revision of IEEE Std 421.5-1992), 1–93.

Deadrick, F., Hawke, R., Scudder, J., Jan 1982. Magrac–a railgun simulation program. IEEE Transactions on Magnetics 18 (1), 94–104.

Doktorcik, C. J., 2011. Modeling and simulation of a hybrid ship power system. Master's thesis, Purdue University.

Hecht, J., April 2018. The ray guns are coming. IEEE Spectrum 55 (4), 24–50.

Huang, K., Cartes, D. A., Srivastava, S. K., 2007. A multiagent-based algorithm for ring-structured shipboard power system reconfiguration. IEEE Transactions on Systems, Man, and Cybernetics, Part C (Applications and Reviews) 37 (5), 1016–1021.

Kuseian, J., 2015. Naval power and energy systems technology development roadmap. Naval Sea Systems Command.

Mills, A. J., Ashton, R. W., 2017. Reduced order multi-rate lqr controllers for a mvdc shipboard electric distribution system with constant power loads. In: Electric Ship Technologies Symposium (ESTS), 2017 IEEE. IEEE, pp. 170–175.

Monti, A., Boroyevich, D., Cartes, D., Dougal, R., Ginn, H., Monnat, G., Pekarek, S., Ponci, F., Santi, E., Sudhoff, S., et al., 2005. Ship power system control: A technology assessment. In: Electric Ship Technologies Symposium, 2005 IEEE. IEEE, pp. 292–297.

O'Rourke, R., 2017. Navy lasers, railgun, and hypervelocity projectile: Background and issues for congress. Tech. rep., Congressional Research Service Washington United States.

Patsios, C., Antonopoulos, G., Prousalidis, J., 2012. Discussion on adopting intelligent power management and

 http://doi.org/10.24868/issn.2631-8741.2018.025

control techniques in integrated power systems of all-electric ships. In: Electrical Systems for Aircraft, Railway and Ship Propulsion (ESARS), 2012. IEEE, pp. 1–6.

Trinklein, E. H., Parker, G. G., McCoy, T. J., Robinett III, R. D., Weaver Jr., W. W., 2018. Reduced order multi-domain modeling of shipboard systems for exergy-based control investigations. In: American Society of Naval Engineers (ANSE), Technology, Ships, and Systems (TTS), 2018. ASNE.

Wilson, D. G., Robinett, R. D., Goldsmith, S. Y., June 2012. Renewable energy microgrid control with energy storage integration. In: International Symposium on Power Electronics Power Electronics, Electrical Drives, Automation and Motion. pp. 158–163.

Zhang, Y., Cramer, A. M., 2017. Market-based control of electric ship power systems. In: Electric Ship Technologies Symposium (ESTS), 2017 IEEE. IEEE, pp. 372–379.

 http://doi.org/10.24868/issn.2631-8741.2018.025